Inorganic Chemistry

Article

pubs.acs.org/IC

Heteroleptic Cyclometalated Iridium(III) Complexes Supported by Triarylborylpicolinate Ligand: Ratiometric Turn-On Phosphorescence Response upon Fluoride Binding

Sanjeev Sharma,[†,§] Hyungjun Kim,[‡,§] Young Hoon Lee,[†] Taewon Kim,[†] Yoon Sup Lee,[‡] and Min Hyung Lee*[,†]

[†]Department of Chemistry and EHSRC, University of Ulsan, Ulsan 680-749, Republic of Korea

[‡]Department of Chemistry, KAIST, Daejeon 305-701, Republic of Korea

Supporting Information

ABSTRACT: Heteroleptic cyclometalated iridium(III) complexes $(C^N)_2Ir(Bpic)$ (**4**–**6**) (C^N = *dfppy* (**4**), *ppy* (**5**), *btp* (**6**)) supported by triarylborylpicolinate (Bpic) ancillary ligand were synthesized and characterized. X-ray diffraction study of **5** confirmed N^O chelation of the Bpic ligand to the iridium center forming an $(C^N)_2Ir$–borane conjugate. While the UV/vis absorption bands of **4**–**6** remained almost unchanged in the low-energy region upon fluoride addition, a ratiometric turn-on phosphorescence response was observed for **4** and **5**. In contrast, the phosphorescence of **6** was little affected by fluoride binding. Experimental and theoretical studies suggest that the LUMO in neutral **4** and **5** is dominated by the Bpic ligand, which makes the weakly emissive $^3ML'CT/^3LL'CT$ (L = C^N; L′ = Bpic) states as the lowest-energy triplet excited state, while the fluoride binding to **4** and **5** induces the highly emissive $^3MLCT/^3\pi\pi^*$ states centered on the $(C^N)_2Ir$ moiety. Thermally induced conversion from the $^3MLCT/^3\pi\pi^*$ to the $^3ML'CT/^3LL'CT$ states is suggested to be responsible for the low-energy weak phosphorescence in **4** and **5**.

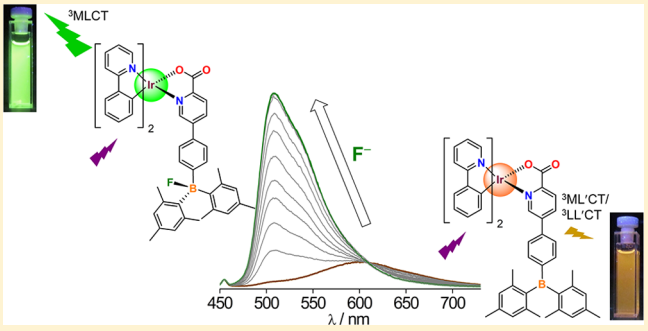

INTRODUCTION

Triarylborane compounds have attracted great attention as receptors for toxic anions such as fluoride and cyanide, because of their high Lewis acidity. It was well established that a strong Lewis acid–base interaction between the boron atom of triarylborane and anions serves as the basis for the detection of small nucleophilic anions in combination with optical changes during anion recognition.[1,2] Most triarylborane receptors utilize optical changes in color,[2−4] absorption, or fluorescence,[5−7] which occur during the binding of an anion to the boron center of triarylboranes. While these methods have enabled simple and easy detection of anions, much attention has also been focused on the phosphorescent sensors based on heavy-metal complexes conjugated with triarylboranes, because of their advantageous photophysical properties, such as large Stokes shifts, long emission lifetimes, and high quantum efficiency. These properties are beneficial for obtaining high signal-to-noise ratios and for easy separation of the signal from undesired fluorescence noise in the medium.[8,9]

Among the various triarylborane-containing transition-metal receptors,[6,9−12] cyclometalated Ir(III)–borane conjugates are of great interest, because of the easy tunability of phosphorescence accomplished by changing the structure of the cyclometalating ligand (C^N), high quantum efficiency, and relatively high stability of $(C^N)_2Ir$ moiety under ambient conditions.[13] In particular, the phosphorescence from the lowest-energy triplet states, such as metal-to-ligand charge transfer (^3MLCT) and ligand-centered transition ($^3\pi\pi^*$ or ^3LC) can be readily modified by anion binding to the triarylborane moiety, thereby enabling facile detection of the anion. For example, fluoride binding to the dimesitylboryl (Mes_2B) moiety attached on a C^N ligand led to the red-shift of the ^3MLCT band by raising the highest occupied molecular orbital (HOMO) level of the conjugate (**I** in Chart 1).[9] Huang and co-workers reported a ratiometric fluoride probe whose phosphorescence centered on the $(C^N)_2Ir$ moiety can be switched to fluorescence of the carbazole containing N^N ancillary ligand after fluoride binding (**II**).[12,14]

However, the borane moieties in the reported Ir(III)–borane conjugates including **I** and **II** are usually linked to a C^N ligand.[9,11,12,14] Although these types of conjugates have shown substantial change of phosphorescence upon fluoride binding, the generation of anionic C^N ligand could reduce the intensity of the $^3MLCT/^3\pi\pi^*$ emission of the $(C^N)_2Ir$ moiety, i.e., it could result in a turn-off response.[9,11] To circumvent this phenomenon, we recently reported "OFF–ON"-type phosphorescent receptors in which a triarylborane moiety was

Received: June 3, 2014
Published: August 4, 2014

   dx.doi.org/10.1021/ic501286m | *Inorg. Chem.* 2014, 53, 8672−8680

Chart 1

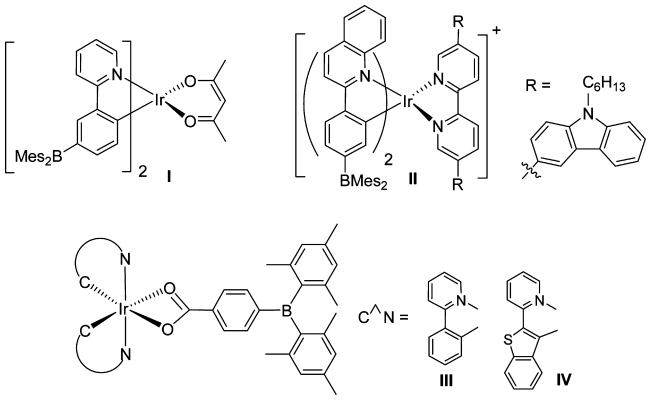

introduced into the LX ancillary ligand of the heteroleptic Ir(III) complexes (**III** and **IV**).[15] It was demonstrated that the neutral conjugates are very weakly emissive, because of photoinduced electron transfer (PET) from the MLCT state of the $(C^N)_2Ir$ moiety to the borane, while anion binding prevented the PET process and minimally affected the photophysical properties of the $(C^N)_2Ir$ moiety. As a result, a "turn-on" response toward fluoride, which is a favored sensing scheme from an analytical point of view,[4,7,16] was observed in these conjugates.

To extend the design principles of the turn-on-type Ir(III)–borane conjugates and to see the impact of ancillary ligand on the photophysical properties of the iridium(III) complex, we further focused on other LX ligand systems bearing triarylboryl groups. Since it turned out that the foregoing 4-membered O^O ligand was rather unstable in anion-abundant conditions, we chose the strong 5-membered N^O chelating ligand as an ancillary ligand backbone. In this study, we designed triarylboryl substituted picolinate ligand (Bpic) and prepared the heteroleptic $(C^N)_2Ir(Bpic)$ complexes with a different C^N ligand, **4**–**6** (C^N = 2-(4,6-difluorophenyl)pyridinato-C^2,N (*dfppy*, **4**); 2-phenylpyridinato-C^2,N (*ppy*, **5**); 2-(2-benzothienyl)-pyridinato-C^2,N (*btp*, **6**)). Depending on the nature of the $(C^N)_2Ir$ moiety, different phosphorescence responses were observed including a ratiometric turn-on change toward fluoride binding. Details of synthesis, photophysical properties, and fluoride binding behavior of **4**–**6** are described with theoretical calculations.

RESULTS AND DISCUSSION

Synthesis and Characterization. The Suzuki–Miyaura coupling reaction of methyl 5-bromo-2-picolinate (**1**)[17] with (4-dimesiylboryl)-phenylboronic acid (**2**)[18] produced the 5-triarylboryl (Mes_2PhB) substituted 2-picolinic acid (BpicH, **3**) in moderate yield (50%) after hydrolysis. Reaction of **3** with the dimeric iridium(III) compounds $[(C^N)_2Ir(\mu\text{-}Cl)_2Ir(C^N)_2]$ (C^N = *dfppy* (**4a**); *ppy* (**5a**); *btp* (**6a**))[19,20] afforded the corresponding heteroleptic $(C^N)_2Ir(Bpic)$ complexes (**4**–**6**) in moderate yield (48%–60%) (Scheme 1). The formation of **4**–**6** was characterized by multinuclear NMR spectroscopy, elemental analysis, and X-ray diffraction. While the ^1H and ^{13}C NMR spectra showed the expected resonances corresponding to the $(C^N)_2Ir$ and Bpic moieties, the ^{11}B NMR signals detected in the region of δ +75 ppm confirmed the presence of the tricoordinate boron center. X-ray diffraction analysis revealed the molecular structure of **5** (see Figure 1 and Table S1 in the Supporting Information). The crystal structure shows that the Bpic ligand is coordinated to the Ir atom via bidentate N^O chelation, forming an Ir(III)-borane conjugate. The B atom in the Bpic moiety adopts a trigonal planar geometry, as judged from the summation of the three C–B–C angles ($\sum_{(C-B-C)}$ = 359.9°). This feature is consistent with the ^{11}B NMR signals. The Ir-centered moiety bears two *ppy* ligands being in a trans disposition of the pyridyl rings, as has usually been observed in other $(ppy)_2Ir(LX)$ complexes including **III**.[15,20,22] The pyridyl and phenylene ring planes in the Bpic moiety form a small dihedral angle of 14.7(4)°, indicating the presence of electronic conjugation over the Bpic ligand. Bond distances and angles around the Ir center are in a similar range to those reported for $(C^N)_2Ir(N^O)$ complexes,[23,24] with a longer Ir–N(Bpic) bond distance (2.163(6) Å) than those of the Ir–N(pyd) bonds (2.029(7) and 2.056(6) Å), because of the strong trans influence of a phenyl group of *ppy* ligand on the Ir–N(Bpic) bond.

Photophysical and Electrochemical Properties. UV/vis and photoluminescence (PL) titrations were carried out with **4**–**6** in aerated THF to examine the optical changes upon fluoride ion binding (Figure 2 and Table 1). All compounds

Scheme 1. Synthesis of $(C^N)_2Ir(Bpic)$ Complexes

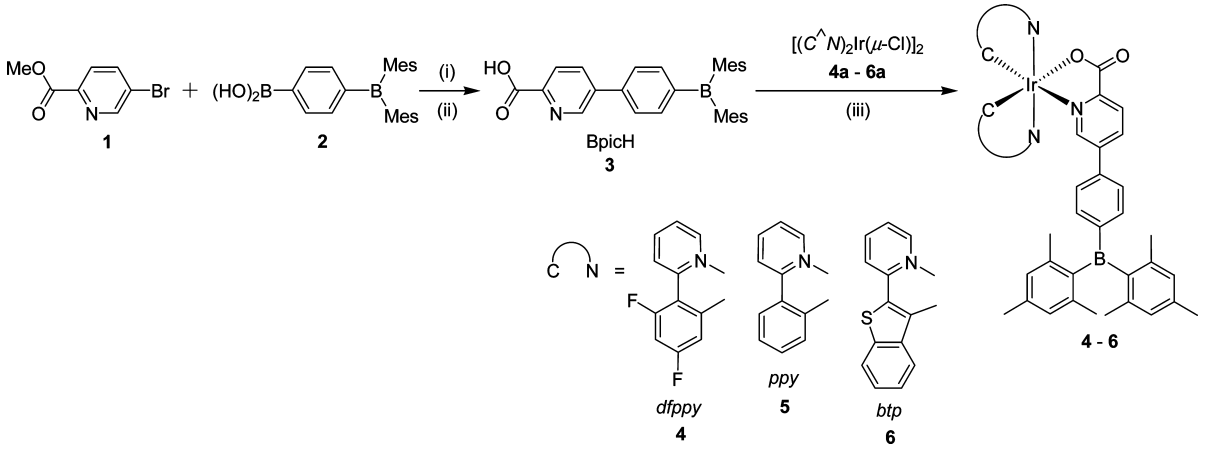

[a]Conditions: (i) $Pd(PPh_3)_4$, Na_2CO_3, toluene/H_2O, 90 °C, 56%. (ii) KOH, MeOH/THF/H_2O, room temperature (rt), 90%. (iii) Na_2CO_3, 2-ethoxyethanol, 120 °C, 55% (**4**), 60% (**5**), and 48% (**6**).

dx.doi.org/10.1021/ic501286m | Inorg. Chem. 2014, 53, 8672–8680

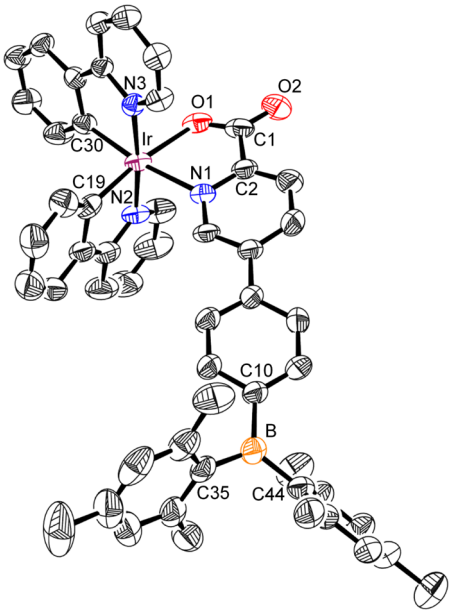

Figure 1. Crystal structure of **5** (40% thermal ellipsoids). The H atoms and solvent molecule (THF) are omitted for clarity. Selected bond lengths: Ir−N(1), 2.163(6) Å; Ir−N(2), 2.029(7) Å; Ir−N(3), 2.056(6) Å; Ir−O(1), 2.165(6) Å; Ir−C(19), 1.988(8) Å; Ir−C(30), 2.016(8) Å; B−C(10), 1.585(12) Å; B−C(35), 1.557(13) Å; and B−C(44), 1.581(12) Å. Selected bond angles: N(2)−Ir−N(3), 173.9(2)°; N(1)−Ir−O(1), 76.4(2)°; N(2)−Ir−C(19), 80.9(3)°; N(3)−Ir−C(30), 80.9(3)°; C(10)−B−C(35), 118.1(7)°; C(10)−B−C(44), 119.3(8)°; and C(35)−B−C(44), 122.5(7)°.

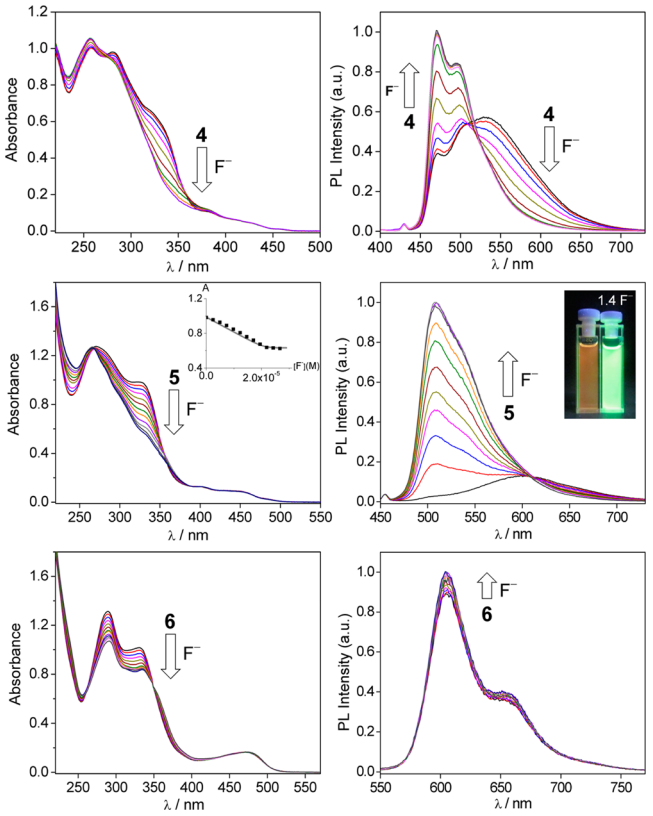

Figure 2. Changes in the UV/vis absorption (left) and PL (right) spectra of **4**−**6** in aerated THF upon addition of Bu_4NF. (Top row) **4** (1.96×10^{-5} M) with 0−1.4 equiv Bu_4NF, λ_{ex} = 380 nm; (middle row) **5** (2.10×10^{-5} M) with 0−1.4 equiv Bu_4NF, λ_{ex} = 400 nm (the left inset shows the absorbance at 325 nm as a function of $[F^-]$; the line corresponds to the binding isotherm calculated with $K = 1.0 \times 10^7$ M^{-1}, and the right inset shows a photograph of the emission color change before (left) and after (right) fluoride addition); (bottom row) **6** (2.00×10^{-5} M) with 0−1.4 equiv Bu_4NF, λ_{ex} = 420 nm.

feature an intense absorption band in the high-energy region (250−370 nm), which was gradually quenched upon the addition of incremental amounts of fluoride. As can be seen from the similar absorption quenching behavior of ligand **3** (Figure S2 in the Supporting Information), this band may be associated with the π(Mes) to π^*(Bpic) intraligand charge transfer (ILCT) transition in the Bpic ligand (see DFT results).[25−27] From the 1:1 binding isotherm (Figures S3 and S4 in the Supporting Information),[26,28] the fluoride binding constant (K) was estimated to be ~10^7 M^{-1} for **4**−**6**. This value is similar to that observed for **3** ($K = 1.2 \times 10^7$ M^{-1}), as well as that of the Mes_2PhB compound ($K = 5.0 \times 10^6$ M^{-1} in THF),[25] having a similar steric environment around the B atom. On the other hand, the lower-energy absorption bands (370−500 nm) exhibit the typical features observed for $(C^N)_2Ir$ moieties. The spin-allowed ^{1}MLCT bands (centered on 380 nm for **4**, 400 nm for **5**, and 474 nm for **6**) and the mixed ^{3}MLCT and $^3\pi\pi^*$ transition (^{3}LC) of the C^N ligands (centered on 427 nm for **4**, 452 nm for **5**, and 474 nm for **6**) are observed in the similar regions found in other $(C^N)_2Ir(LX)$ complexes (LX = picolinate,[23,24,29,30] acetylacetonate,[20,22] benzoate,[15,31]).

In particular, these bands remained almost unchanged upon fluoride addition. This indicates that the fluoride binding at the Bpic ligand has little effect on the electronic structure of the $(C^N)_2Ir$ moiety, implying the retention of the photophysical properties of the $(C^N)_2Ir$ moieties even after fluoride complexation.

In contrast to the absorption features, the PL spectra of neutral **4**−**6** exhibit quite different emission behaviors, compared to other $(C^N)_2Ir(LX)$ complexes (Figure 2, right). Compound **4** shows a broad emission band centered at 533 nm with small peaks at 471 and 501 nm. Upon the addition of fluoride, the intensity of the band at 533 nm gradually decreases, while the higher-energy bands at 471 and 501 nm grow larger. The final emission band, after the addition of more than 1 equiv of fluoride, quite closely resembles those of the $(dfppy)_2Ir(LX)$ (LX = picolinate, acetylacetonate) complexes,[23,29,32] indicating that the emission originates from the admixture of the ^{3}MLCT and $^3\pi\pi^*$ states of the $(dfppy)_2Ir$ moiety.[23,29,33] This result suggests that the formation of $[\mathbf{4}F]^-$ activates $(dfppy)_2Ir$-centered phosphorescence. A similar, but more pronounced turn-on phosphorescence was also observed from PL titration of **5**. While neutral **5** exhibits a weak and broad emission centered at 599 nm, the addition of fluoride switches on a new emission at 509 nm, with an 8-fold increase in the emission peak intensity after the addition of 1 equiv of fluoride. This was also accompanied by an increase in the quantum efficiency (Φ_{PL}) of **5** from 0.005 to 0.024 after fluoride complexation in aerated THF. The shape and position of the emission band are very similar to those observed for $(ppy)_2Ir(LX)$ complexes[20,22] including $(ppy)_2Ir(pic)$,[24,30] indicating that the new emission can be assigned to the $(ppy)_2Ir$-centered phosphorescence with the ^{3}MLCT mixed with $^3\pi\pi^*$ state in character. The turn-on response of **5** toward fluoride binding can also be vividly observed from its emission color change from weak orange to bright greenish under UV light (Figure 2, right inset). In contrast, the neutral **6** exhibits a red

dx.doi.org/10.1021/ic501286m | Inorg. Chem. 2014, 53, 8672−8680

Table 1. Photophysical and Electrochemical Data for 3−6 and Fluoride Adducts

compound	λ_{abs} (nm)[a]	λ_{em} (nm)[a] 298 K	λ_{em} (nm)[a] 77 K	Φ_{PL}[a,b]	E_{ox} (V)[c]	E_{red} (V)[c]
3 (BpicH)	291 (20.2), 328 (18.3)	426	397, 488, 521			
4 (*dfppy*)	258 (50.1), 280 (49.0), 322 (32.6), 380 (5.4), 427 (2.2)	471, 501, 533	459, 491, 515	0.041	0.91[d]	−1.89,[d] −2.16[e]
[**4**F]$^-$	257 (53.7), 278 (48.0), 380 (5.8), 427 (2.2)	471, 497	459, 491, 518	0.036		−2.25[d]
5 (*ppy*)	270 (60.5), 326 (46.6), 400 (6.0), 452 (4.2)	599	491, 525	0.005	0.58[d]	−1.94,[d] −2.23[e]
[**5**F]$^-$	266 (60.0), 330 (26.8), 400 (6.0), 452 (4.0)	509	490, 524	0.024		−2.32[d]
6 (*btp*)	289 (65.6), 331 (50.8), 474 (8.2)	605, 655	591, 610, 651	0.003	0.50,[d] 1.06[d]	−1.89,[d] −2.18[e]
[**6**F]$^-$	291 (53.5), 334 (41.8), 474 (8.4)	605, 655	591, 610, 651	0.003		−2.21[d]

[a]Measured in aerated THF (~10^{-5} M). The values given in parentheses are the corresponding ε values (× 10^3 M^{-1} cm^{-1}). [b]*fac*-Ir(*ppy*)$_3$ in degassed THF (Φ_{PL} = 0.97)[21] as a standard. [c]Measured in CH_3CN at a scan rate of 100 mV/s, with reference to a Fc/Fc^+ couple. [d]Reversible. [e]Irreversible.

emission centered at 605 and 655 nm, as typically observed in the (*btp*)$_2$Ir(LX) complexes,[22,34] but the addition of fluoride does not cause a noticeable increase in the emission intensity. This finding suggests that the lowest-energy excited states of both **6** and [**6**F]$^-$ are dominated by the $^3\pi\pi^*$ state of the (*btp*)$_2$Ir moiety.[22]

The observed turn-on process upon fluoride binding in **4** and **5** can be described as "ratiometric". This is somewhat different from that observed for compounds **III** and **IV** (Chart 1), in which the "true" turn-on process occurred by blocking a PET process upon fluoride binding.[15] Furthermore, the emission change did not noticeably occur in the red conjugate **6**. To elucidate the origin of the emission change, we first examined the electrochemical properties of **4**−**6** by cyclic voltammetry (see Table 1 and Figure 3). Compounds **4**−**6** undergo

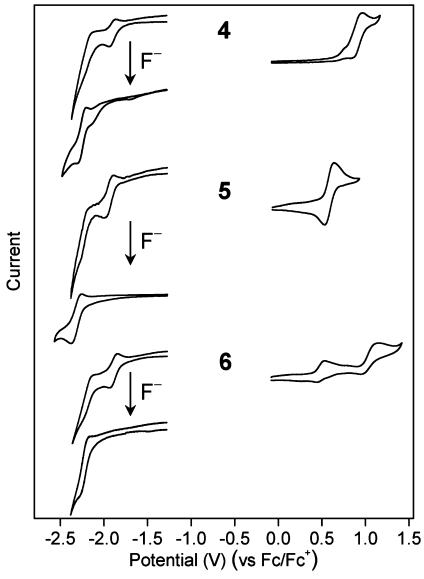

Figure 3. Cyclic voltammograms of **4**−**6** (1 mM in MeCN, scan rate = 100 mV/s) before and after the addition of 2 equiv Bu_4NF.

reversible oxidation at 0.91, 0.58, and 0.50 V, respectively, which is in accordance with the electronic effect of the C^N ligand on the d_π(Ir) orbitals. While the oxidation potential of **4** is very similar to that of (*dfppy*)$_2$Ir(pic) (0.89−0.92 V),[23,35] the oxidation in **5** and **6** is anodically shifted, in comparison to that of (*ppy*)$_2$Ir(acac) (0.41 V)[33] and (*btp*)$_2$Ir(acac) (0.36 V)[36] complexes, respectively, likely due to the stronger ligand effect of Bpic than the acac ligand. On the other hand, compounds **4**−**6** display a reversible first reduction at −1.89, −1.94, and −1.89 V, respectively, and a weak second reduction at the lower potential region. The similar first reduction potentials of all of the compounds indicate a common origin of the reduction processes. In combination with the highly anodically shifted first reduction compared to that of the usual (C^N)$_2$Ir(LX) complexes (between −2.4 V and −2.6 V), this result strongly suggests that the reduction occurs not on the C^N ligand, but on the Bpic ligand. In order to confirm the Bpic-centered reduction in **4**−**6**, we further investigated the reduction behavior in the presence of fluoride (Figure 3). Upon fluoride addition, all compounds show a dramatic change in reduction leading to large cathodic shifts of the reduction peaks. The newly formed reduction closely resembles the C^N-centered reduction of usual (C^N)$_2$Ir(LX) complexes. This result clearly confirms the Bpic-centered first reduction in **4**−**6**. These electrochemical results suggest that, while the metal center contributes to the HOMO in **4**−**6**, the lowest unoccupied molecular orbital (LUMO) is dominated by the Bpic ligand.

Next, the triplet energy of the Bpic ligand was determined to examine whether the broad low-energy emission in **4** and **5** is involved with the $^3\pi\pi^*$ state of the Bpic ligand (^{3}L′X). As shown in Figure 4, the PL spectra of **3** at 77 K exhibit

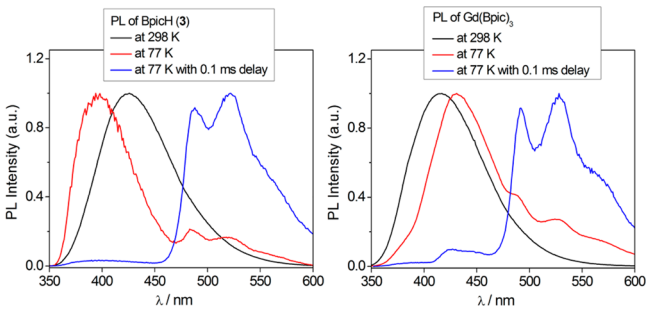

Figure 4. Photoluminescence (PL) spectra of BpicH (**3**) (left) and in situ Gd(Bpic)$_3$ (right) in THF.

structured phosphorescence typical of the emission from the $^3\pi\pi^*$ state. The lowest triplet state (T_1) energy of **3** can be deduced from the highest energy peak (E_{0-0}) at 488 nm, which afforded a T_1 energy of 2.54 eV. Similarly, the phosphorescence spectra of in-situ-generated Gd(Bpic)$_3$ solution were also obtained, from which a similar T_1 state energy of Bpic (2.52 eV) was determined (Figure 4, right). However, it is notable that the T_1 energy of the Bpic ligand is far from the phosphorescence bands of **4** and **5** (Figure 2). This result indicates that the ^{3}L′X state of the Bpic ligand is not responsible for the low-energy emission observed in **4** and **5**. Since the emissions at 533 and 599 nm in **4** and **5**, respectively, are lower in energy than the ^{3}MLCT/$^3\pi\pi^*$ states of the

dx.doi.org/10.1021/ic501286m | Inorg. Chem. 2014, 53, 8672−8680

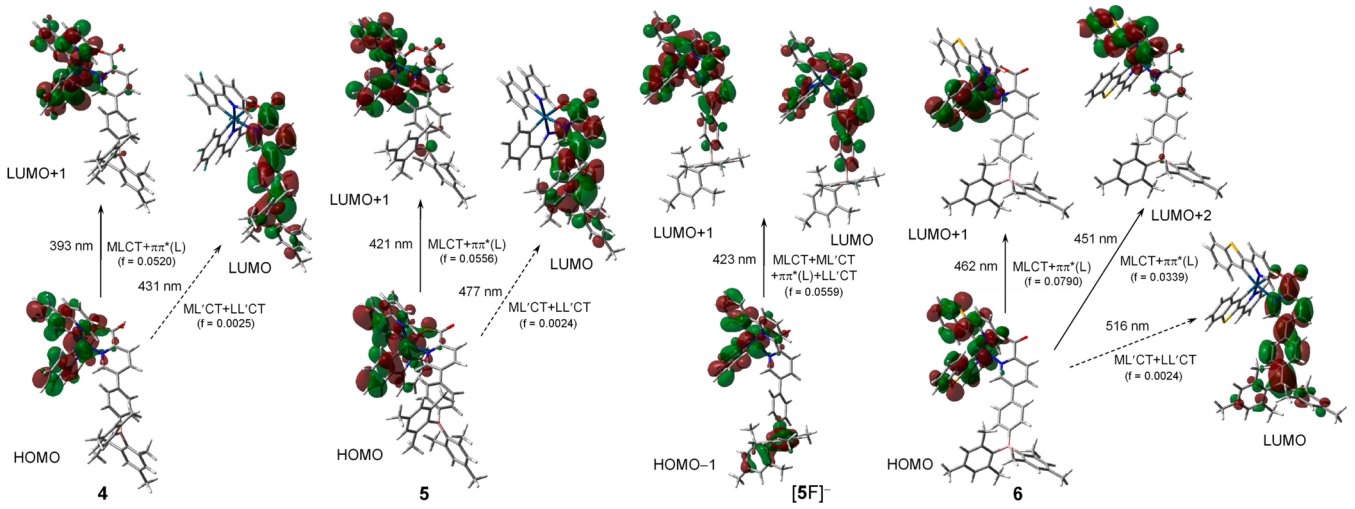

Figure 5. Frontier molecular orbitals of **4**–**6** and $[\mathbf{5F}]^-$ at their ground state (S_0) optimized geometries, and the lower-energy electronic transition from TD-DFT calculation (L = C^N; L′ = Bpic ligand; isovalue = 0.04).

$(C^N)_2Ir$ moiety, and since the LUMO is localized on the Bpic ligand (L′), it can be suggested that the emission originates from the triplet state associated with the Bpic ligand, such as ^{3}ML′CT/^{3}LL′CT (ligand-to-ligand charge transfer). The broad emission feature also supports CT transition in nature. Furthermore, since the HOMO energy levels of **4** and **5** are affected by the electronic properties of the C^N ligand, which, in turn, influences the band gap, the more electron-withdrawing *dfppy*-containing **4** would have a higher emission energy than **5** (533 nm for **4** vs 599 nm for **5**). However, upon fluoride binding, LUMO is no longer dominated by the Bpic ligand, as shown in the electrochemical reduction; therefore, the C^N ligand will govern the excited-state properties of the fluoride adduct. Consequently, the emission from the ^{3}MLCT/$^3\pi\pi^*$ states of $(C^N)_2Ir$ moiety is restored (Figure 2). In contrast, because of the low-lying $^3\pi\pi^*$ state of the $(btp)_2Ir$ moiety, the possible conversion to the ^{3}ML′CT/^{3}LL′CT states could be inefficient in **6**, giving rise to almost no change in the phosphorescence before and after fluoride binding.

The change in PL spectra of **5** was further examined in the presence of various anions (see Figure S5 in the Supporting Information). Because of the incompatibility of **5** with an aqueous medium, the binding experiments were carried out in THF. While the weak phosphorescence band of **5** was not significantly affected in the presence of other anions (2 equiv), such as Cl^-, Br^-, I^-, NO_3^-, ClO_4^-, and HSO_4^-, the addition of OAc^- led to a moderate increase in the emission intensity, as usually observed in the triarylborane-based receptors. This result indicates high selectivity of **5** toward fluoride.

Theoretical Calculations. To gain insight into the electronic transition and phosphorescence change in **4**–**6**, TD-DFT calculations were carried out at the ground (S_0) and lowest-energy triplet excited state (T_1) optimized geometries (see Figures 5 and 6). Orbital analyses on the ground-state structures show that, although the HOMOs are mainly located on the d_π(Ir) and π(C^N) orbitals in **4**–**6**, LUMOs are localized on the Bpic ligand, which bears extended conjugation from picolinate π^* to the empty p_π(B) orbital. However, the HOMO–LUMO transition, which could be characterized by ML′CT/LL′CT transition, hardly takes place, judging from its very low oscillator strength for all complexes (f = 0.0024–0.0025). Indeed, the solutions of **4**–**6** did not show a noticeable

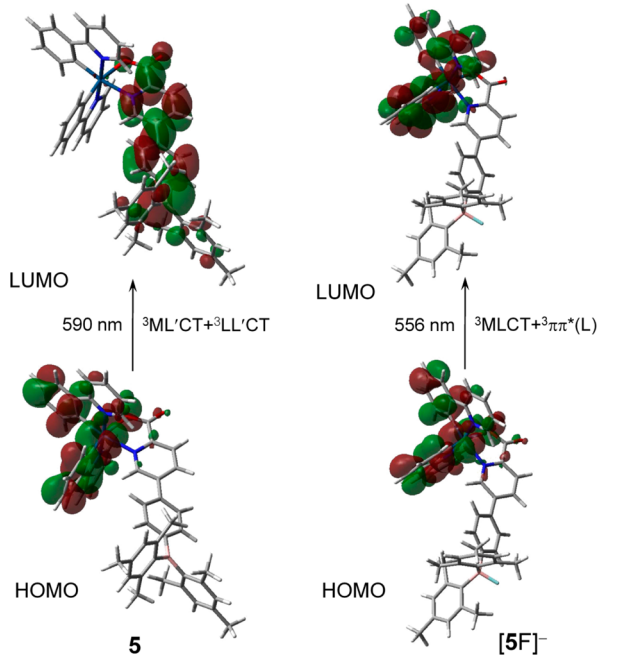

Figure 6. Frontier molecular orbitals of **5** and $[\mathbf{5F}]^-$ at their first excited triplet state (T_1) optimized geometries, and the lowest-energy electronic transition from TD-DFT calculation (L = *ppy*; L′ = Bpic ligand; isovalue = 0.04).

spectral change in the low-energy region before and after fluoride addition, supporting the little involvement of Bpic in the low-energy absorption process. In contrast, the HOMO–LUMO+1 transition, which can be mainly assignable to the ^{1}MLCT transition, is apparently observed as a low-energy electronic transition. Note that the LUMO+1 has a major contribution from the π^*(C^N) orbital. This feature is very similar to those observed for usual $(C^N)_2Ir(LX)$ complexes, and the computed absorption wavelength correlates well with the experimentally observed absorption bands (Figure 5 versus Figure 2 and Table 1). To examine the change in the electronic transition after the binding of fluoride to the B atom of the Bpic ligand, we further optimized the structure of the fluoride adduct, $[\mathbf{5F}]^-$ (Figure 5). The lowest-energy absorption in

dx.doi.org/10.1021/ic501286m | Inorg. Chem. 2014, 53, 8672–8680

$[\mathbf{5F}]^-$ is characterized by HOMO−1 → LUMO (43.8%) and HOMO−1 → LUMO+1 (36.3%) transitions. While HOMO−1 resides on the $(ppy)_2$Ir moiety mixed with a contribution from the Mes groups, LUMO and LUMO+1 are delocalized over the *ppy* ligand and picolinate fragment with no contribution from the B atom. This feature is in parallel with the electrochemical reduction of **5** in the presence of fluoride (Figure 3). Moreover, the fact that fluoride binding to **5** did not result in a spectral change in the low-energy absorption region supports that the transition in $[\mathbf{5F}]^-$ is mainly MLCT in nature, among the possible transitions. It is noteworthy that the computed oscillator strength of the low-energy transition in **5** (f = 0.0556) is very similar to that in $[\mathbf{5F}]^-$ (f = 0.0559).

Finally, TD-DFT calculations at the T_1 optimized geometry of **5** and $[\mathbf{5F}]^-$ were performed to examine the turn-on phosphorescence change (Figure 6). In **5**, the lowest-energy triplet excited state (T_1) is involved with the HOMO → LUMO (94.7%) transition, assignable to be ^{3}ML′CT/^{3}LL′CT in character. The computed phosphorescence wavelength of **5** matches well with the experimentally observed band (590 nm vs 599 nm). While the LUMO in the T_1 state of **5** is localized on the Bpic ligand, similar to the S_0 state structure, the LUMO in the T_1 state of $[\mathbf{5F}]^-$ is dominated by the π^* orbital of the *ppy* ligand, because of occupation of the p_π(B) orbital in **5** by fluoride. Thus, the lowest-energy transition is changed to the ^{3}MLCT/$^3\pi\pi^*$ states centered on the $(ppy)_2$Ir moiety in $[\mathbf{5F}]^-$. Although the difference in the computed phosphorescence wavelength between **5** and $[\mathbf{5F}]^-$ ($\Delta\lambda_{em}$ = ca. 34 nm, 1040 cm^{-1}) is smaller than the observed experimental difference ($\Delta\lambda_{em}$ = ca. 90 nm, 2950 cm^{-1}), it is obvious that the phosphorescence of **5** is substantially blue-shifted, and may gain large emission intensity from the highly emissive ^{3}MLCT/$^3\pi\pi^*$ states upon fluoride binding.

Based on the foregoing experimental and theoretical results, the turn-on phosphorescence process in **4** and **5** upon fluoride binding could be proposed as shown in Figure 7. Upon

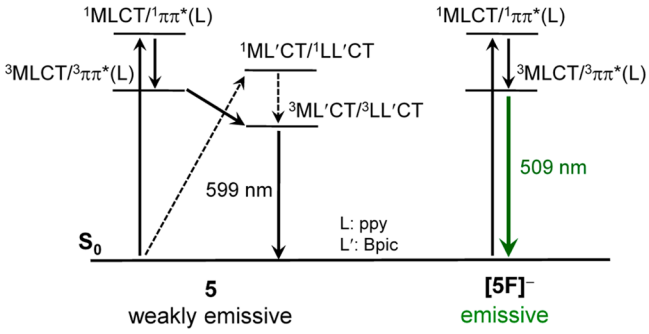

Figure 7. Proposed energy level diagram and phosphorescence process in **5** and $[\mathbf{5F}]^-$.

photoexcitation of **5**, the singlet excited states of the $(ppy)_2$Ir moiety, such as ^{1}MLCT/$^1\pi\pi^*$, undergo intersystem crossing to their lower-energy triplet excited states (^{3}MLCT/$^3\pi\pi^*$). These states then undergo rapid conversion to the lowest-lying ^{3}ML′CT/^{3}LL′CT states, leading to weak phosphorescence at 599 nm. Since dual emission was observed for **4** at room temperature (rt) (Figure 2), the ^{3}MLCT/$^3\pi\pi^*$ and ^{3}ML′CT/^{3}LL′CT states appear to be weakly coupled to each other. Comparison of the PL spectra of **4** and **5** obtained at 77 K with those at rt clearly shows that the phosphorescence from the ^{3}MLCT/$^3\pi\pi^*$ states of the $(C\text{^}N)_2$Ir moieties is dominating at 77 K in both complexes (see Figure S6 in the Supporting Information and Table 1). This result strongly suggests that the population of the ^{3}ML′CT/^{3}LL′CT states is thermally induced, as similarly shown in tris(pyridylazolate) iridium complexes reported by Chou and co-workers.[37] Furthermore, because the low-energy electronic transition mediated by the Bpic ligand was hardly observable in the absorption spectra and the oscillator strength of the transition was also very low, it can be assumed that a deactivation pathway of the excited states through direct excitation to the singlet manifold of ^{1}ML′CT/^{1}LL′CT, followed by intersystem crossing to the T_1 (^{3}ML′CT/^{3}LL′CT) state, will not be allowed (dashed arrows in Figure 7). In contrast, the ^{3}MLCT/$^3\pi\pi^*$ states of the $(ppy)_2$Ir moiety solely constitute the T_1 state of $[\mathbf{5F}]^-$. Therefore, the $(ppy)_2$Ir-centered strong phosphorescence can be observed at a high-energy region (509 nm), demonstrating the ratiometric, as well as turn-on phosphorescence change of **5** upon fluoride binding (Figure 7, right).

CONCLUSION

Heteroleptic $(C\text{^}N)_2Ir^{III}$–borane conjugates (C^N = *dfppy* (**4**), *ppy* (**5**), *btp* (**6**)) supported by the triarylborylpicolinate (Bpic) ancillary ligand were synthesized and characterized. While **4** and **5** showed a ratiometric turn-on phosphorescence response toward fluoride, the phosphorescence of **6** was little affected. It was demonstrated by experimental and theoretical studies that the LUMO is dominated by the Bpic ligand in neutral **4** and **5**, which puts the weakly emissive ^{3}ML′CT/^{3}LL′CT (L = C^N; L′ = Bpic) states as the lowest-energy triplet excited state, while the fluoride binding induces the highly emissive ^{3}MLCT/$^3\pi\pi^*$ (L = C^N) states centered on the $(C\text{^}N)_2$Ir moiety. Thermally induced conversion from the ^{3}MLCT/$^3\pi\pi^*$ to the ^{3}ML′CT/^{3}LL′CT states was suggested to be responsible for the low-energy weak phosphorescence in **4** and **5**. The results in this study could be useful for designing highly sensitive ratiometric and/or turn-on phosphorescence sensors for fluoride.

EXPERIMENTAL SECTION

General Considerations. All operations were performed under an inert nitrogen atmosphere using standard Schlenk and glovebox techniques. Anhydrous grade solvents (Aldrich) were dried by passing them through an activated alumina column and stored over activated molecular sieves (5 Å). Spectrophotometric-grade THF (Aldrich) was used as received. Commercial reagents were used without any further purification after purchasing from Aldrich (dimesitylboron fluoride (Mes_2BF), *n*-BuLi (2.5 M solution in *n*-hexanes), 2-ethoxyethanol, Na_2CO_3, tetra-*n*-butylammonium fluoride trihydrate (TBAF), Gd-$(NO_3)_3\cdot 6H_2O$), Strem ($Pd(PPh_3)_4$, iridium(III) chloride hydrate), and Alfa Aesar (5-bromopyridine-2-carboxylic acid). Methyl 5-bromopyridine-2-carboxylate (**1**),[17] 4-(dimesitylboryl)-phenylboronic acid (**2**),[18] and $[(C\text{^}N)_2Ir(\mu\text{-}Cl)]_2$ (C^N = 2-(4,6-difluorophenyl)pyridinato-C^2,N (*dfppy*, **4a**); 2-phenylpyridinato-C^2,N (*ppy*, **5a**); 2-(2-benzothienyl)-pyridinato-C^2,N (*btp*, **6a**)) were analogously synthesized according to the reported procedures.[19,20] Deuterated solvents from Cambridge Isotope Laboratories were used. NMR spectra were recorded on a Bruker 300 AM spectrometer (300.13 MHz for ^{1}H, 75.48 MHz for ^{13}C, 96.29 MHz for ^{11}B) at ambient temperature. Chemical shifts are given in ppm, and are referenced against external Me_4Si (^{1}H, ^{13}C) and $BF_3\cdot Et_2O$ (^{11}B). Elemental analyses were performed on an EA1110 (FISONS Instruments) by the Environmental Analysis Laboratory at KAIST. Mass spectrum was obtained using a JEOL JMS700 high-resolution FAB-mass spectrometer (HR FAB-MS) at the Korea Basic Science Institute (Daegu, Korea). UV/vis and PL spectra were recorded on a Varian Cary 100 and a Horiba

dx.doi.org/10.1021/ic501286m | Inorg. Chem. 2014, 53, 8672−8680

FluoroMax-4P spectrophotometer, respectively. Cyclic voltammetry measurements were performed using an AUTOLAB/PGSTAT101 system.

*Synthesis of 5-(4-(Dimesitylboryl)phenyl)-2-picolinic acid (BpicH, **3**).* A mixture of **1** (0.22 g, 1.0 mmol), **2** (0.41 g 1.1 mmol), Na_2CO_3 (0.42 g, 4.0 mmol), and $Pd(PPh_3)_4$ (0.058 g, 5 mol %) in toluene/H_2O (v/v 3:1, 9 mL) was heated to 90 °C under N_2 overnight. After cooling to room temperature, the mixture was extracted with ethyl acetate (3 × 10 mL). The organic layer was concentrated and purified by column chromatography (silica gel, *n*-hexane/EtOAc: 5/1). Evaporation of the solvent followed by drying under vacuum gave white solid of methyl 5-(4-(dimesitylboryl)phenyl)-2-picolinate (BpicMe). Yield: 0.26 g, 56%. ^{1}H NMR ($CDCl_3$): δ 9.00 (s, 1H, py−C*H*), 8.21 (d, *J* = 8.1 Hz, 1H, py−C*H*), 8.08 (d, *J* = 8.1 Hz, 1H, py−C*H*), 7.60 (m, 4H, Ph−C*H*), 6.82 (s, 4H, Mes−C*H*), 4.02 (s, 3H, CO_2CH_3), 2.30 (s, 6H, Mes−CH_3), 2.00 (s, 12H, Mes−CH_3).

The obtained methyl ester (0.25 g, 0.54 mmol) was dissolved in MeOH/THF/H_2O (15 mL/15 mL/2 mL) mixture and 3 equiv of KOH was added. After stirring overnight at room temperature, the solvent was removed under reduced pressure. The residue was dissolved in H_2O, acidified with 2 M HCl, and extracted with ethyl acetate (30 mL). The organic layer was dried over $MgSO_4$ and solvent was removed under reduced pressure. Drying under vacuum gave a white solid of **3**. Yield: 0.22 g, 90%. ^{1}H NMR ($CDCl_3$): δ 8.91 (s, 1H, py−C*H*), 8.30 (d, *J* = 8.1 Hz, 1H, py−C*H*), 8.19 (d, *J* = 8.1 Hz, 1H, py−C*H*), 7.62 (m, 4H, Ph−C*H*), 6.83 (s, 4H, Mes−C*H*), 2.30 (s, 6H, Mes−CH_3), 2.00 (s, 12H, Mes−CH_3). ^{13}C NMR ($CDCl_3$): δ 164.6 (COO), 147.0, 146.7, 145.2, 141.6, 141.0, 140.8, 139.2, 138.9, 137.3, 137.2, 128.5, 127.0, 124.6, 23.6 (Mes-CH_3), 21.4 (Mes-CH_3). ^{11}B NMR ($CDCl_3$): δ +77.6 (br s). HR MS: Calcd for *m*/*z* ($[M + H]^+$): 448.2448. Found: 448.2453.

*Synthesis of (dfppy)$_2$Ir(Bpic) (**4**).* The dimeric iridium(III) complex **4a** (0.100 g, 0.08 mmol), ligand **3** (0.092 g, 0.21 mmol), and Na_2CO_3 (0.087 g, 0.82 mmol) were stirred in degassed 2-ethoxyethanol (10 mL) at 120 °C for 20 h. After cooling to room temperature, the solvent was removed under reduced pressure to get yellow solid. It was dissolved in toluene (20 mL) and filtered, affording bright yellow solution. The solution was concentrated to ca. 1 mL and hexane was added to precipitate the yellow solid, which was filtered and washed several times with *n*-hexane. Drying under vacuum afforded yellow powder **4**, which was recrystallized from CH_2Cl_2/*n*-hexane. Yield: 0.092 g, 55%. ^{1}H NMR (CD_2Cl_2): δ 8.71 (d, *J* = 5.7 Hz, 1H, *dfppy*-py−C*H*), 8.26 (m, 4H, *dfppy*-py−C*H*), 8.05 (s, 1H, Bpic-py−C*H*), 7.81 (m, 2H, Bpic-py−C*H*), 7.55 (m, 3H, *dfppy*-py−C*H* and Bpic-Ph−C*H*), 7.37 (d, *J* = 8.1 Hz, 2H, Bpic-Ph−C*H*), 7.22 (t, *J* = 6.6 Hz, 1H, *dfppy*-py−C*H*), 7.03 (t, *J* = 6.9 Hz, 1H, *dfppy*-py−C*H*), 6.83 (s, 4H, Bpic-Mes−C*H*), 6.48 (m, 2H, *dfppy*-Ph−C*H*), 5.86 (d, 1H, *J* = 8.7 Hz, *dfppy*-Ph−C*H*), 5.63 (d, 1H, *J* = 8.7 Hz, *dfppy*-Ph−C*H*), 2.29 (s, 6H, Mes-CH_3), 1.96 (s, 12H, Mes-CH_3). ^{13}C NMR (CD_2Cl_2): δ 172.8 (COO), 165.6, 164.6, 164.2, 151.9, 150.9, 149.1, 148.9, 141.1 (B-C_{Mes}), 139.6, 138.9, 138.1, 137.6, 136.9, 128.9, 128.7, 126.7, 123.5, 123.3, 114.9, 98.2, 23.7 (Mes-CH_3), 21.4 (Mes-CH_3). ^{11}B NMR ($CDCl_3$): δ +75.4 (br s). Anal. Calcd for $C_{52}H_{41}BF_4N_3O_2Ir$: C, 61.30; H, 4.06; N, 4.12. Found: C, 61.14; H, 4.00; N, 4.03.

*Synthesis of (ppy)$_2$Ir(Bpic) (**5**).* **5** was prepared in a similar manner as described for **4** using **5a** (0.100 g, 0.093 mmol), **3** (0.104 g, 0.23 mmol), and Na_2CO_3 (0.098 mg, 0.93 mmol). The resulting orange powder was washed several times with *n*-hexane and recrystallized from CH_2Cl_2/*n*-hexane. Yield: 0.11 g, 60%. Single crystals suitable for X-ray difffraction studies were obtained by slow evaporation of THF/MeOH solution of **5**. ^{1}H NMR (CD_2Cl_2): δ 8.73 (d, *J* = 4.8 Hz, 1H, *ppy*-py−C*H*), 8.29 (d, *J* = 7.8 Hz, 1H, Bpic-py−C*H*), 8.16 (d, *J* = 6.3 Hz, 1H, Bpic-py−C*H*), 8.04 (s, 1H, Bpic-py−C*H*), 7.94 (d, *J* = 8.1 Hz, 1H, *ppy*-py−C*H*), 7.87 (d, *J* = 7.8 Hz, 1H, *ppy*-py−C*H*),7.69 (m, 5H, *ppy*-py−C*H* and ppy-Ph−C*H*), 7.49 (d, *J* = 8.1 Hz, 2H, Bpic-Ph−C*H*), 7.32 (d, *J* = 8.1 Hz, 2H, Bpic-Ph−C*H*), 7.17 (t, *J* = 5.7 Hz, 1H, *ppy*-py−C*H*), 6.95 (m, 3H, *ppy*-Ph−C*H*), 6.77 (m, 6H, *ppy*-Ph−C*H* and Bpic-Mes−C*H*), 6.40 (d, *J* = 6.9 Hz, 1H, *ppy*-Ph−C*H*), 6.23 (d, *J* = 6.9 Hz, 1H, *ppy*-Ph−C*H*), 2.30 (s, 6H, Mes−CH_3), 1.96 (s, 12H, Mes−CH_3). ^{13}C NMR (CD_2Cl_2): δ 169.1 (COO), 149.3, 148.9, 144.9, 141.1 (B-C_{Mes}), 139.6, 138.5, 137.9, 137.8, 137.5, 136.0, 132.9, 132.8, 130.4, 129.9, 128.7, 128.5, 126.6, 124.9, 124.6, 123.0, 122.0, 121.8, 119.6, 119.2, 23.6 (Mes-CH_3), 21.4 (Mes-CH_3). ^{11}B NMR ($CDCl_3$): δ +75.8 (br s). Anal. Calcd for $C_{52}H_{45}BN_3O_2Ir$: C, 65.95; H, 4.79; N, 4.44. Found: C, 65.88; H, 5.19; N, 4.11.

*Synthesis of (btp)$_2$Ir(Bpic) (**6**).* **6** was prepared in a similar manner as described for **4** using **6a** (0.100 g, 0.077 mmol), **3** (0.086 g, 0.19 mmol), and Na_2CO_3 (0.082 g, 0.77 mmol). The resulting orange-red powder was washed several times with *n*-hexane and reprecipitated from CH_2Cl_2/*n*-hexane. Yield: 0.078 g, 48%. ^{1}H NMR (CD_2Cl_2): δ 8.74 (d, *J* = 5.7 Hz, 1H, *btp*-py−C*H*), 8.27 (d, *J* = 8.1 Hz, 1H, Bpic-py−C*H*), 8.16 (d, *J* = 8.1 Hz, 1H, Bpic-py−C*H*), 7.93 (s, 1H, Bpic-py−C*H*), 7.76 (m, 6H, *btp*-py−C*H*), 7.55 (d, *J* = 5.4 Hz, 1H, *btp*-py−C*H*), 7.46 (d, *J* = 7.8 Hz, 2H, Bpic-Ph−C*H*), 7.26 (d, *J* = 8.1 Hz, 2H, Bpic-Ph−C*H*), 7.10 (m, 3H, *btp*-benzothio−C*H*), 6.85 (m, 7H, Bpic-Mes−C*H* and *btp*-benzothio−C*H*), 6.24 (d, *J* = 7.8 Hz, 1H, *btp*-benzothio−C*H*), 6.04 (d, *J* = 8.1 Hz, 1H, *btp*-benzothio−C*H*), 2.29 (s, 6H, Mes-CH_3), 1.92 (s, 12H, Mes-CH_3). ^{13}C NMR ($CDCl_3$): δ 173.2 (COO), 166.4, 164.9, 150.4, 150.0, 149.3, 147.8, 146.9, 146.7, 146.1, 145.9, 142.8, 142.7, 141.5, 140.9, 140.8, 139.3, 138.7, 138.6, 137.5, 137.3, 136.4, 136.3, 134.7, 128.4, 126.3, 125.8, 125.7, 125.5, 125.1, 124.2, 123.8, 123.3, 122.9, 119.9, 119.8, 119.4, 118.5, 23.6 (Mes-CH_3), 21.4 (Mes-CH_3). ^{11}B NMR (CD_2Cl_2): δ +75.4 (br s). Anal. Calcd for $C_{56}H_{45}BN_3O_2S_2Ir$: C, 63.50; H, 4.28; N, 3.97. Found: C, 62.44; H, 4.34; N, 3.78. Attempts to obtain a satisfactory elemental analysis data for **6** failed, because of poor crystallinity.

In Situ Preparation of Gd(Bpic)$_3$ Solution. An ethanolic solution of **3** (0.025 g, 0.056 mmol, 4 mL) was adjusted to a pH of 7.5 by adding aqueous NaOH and stirred for 1 h. To this clear solution, $Gd(NO_3)_3 \cdot 6H_2O$ (0.008 g, 0.018 mmol) in ethanol (2 mL) was added and stirred overnight. After evaporation of solvent, the white residue was dissolved in THF. The diluted solution (ca. ~10^{-5} M) was used for PL measurements.

X-ray Crystallography. Single crystals of **5** with suitable size and quality was coated with Paratone oil and mounted onto a glass capillary. The crystallographic measurements were performed using a Bruker Apex II-CCD area detector diffractometer, with graphite-monochromated Mo Kα radiation (λ = 0.71073 Å). The structure was solved by direct methods and all nonhydrogen atoms were subjected to anisotropic refinement by full-matrix least-squares on F^2, using the SHELXTL/PC package.[38] Hydrogen atoms were placed at their geometrically calculated positions and were refined riding on the corresponding carbon atoms with isotropic thermal parameters. The detailed crystallographic data are given in Table S1 in the Supporting Information.

UV/vis Absorption and PL Titration Experiments. UV/vis absorption and PL measurements were performed in aerated THF with a 1 cm quartz cuvette. Typically, a solution of compound (ca. 2.0 × 10^{-5} M, 3.0 mL) was titrated with incremental amounts of fluoride. The absorbance data obtained were fitted to a 1:1 binding isotherm to evaluate the binding constant (*K*). Quantum efficiencies were measured with reference to that of *fac*-Ir(*ppy*)$_3$ in THF (Φ_{PL} = 0.97).[21] The detailed conditions are given in Table 1.

Cyclic Voltammetry. Cyclic voltammetry measurements were carried out in CH_3CN with a three-electrode cell configuration consisting of platinum working electrodes and counter electrodes and a $Ag/AgNO_3$ (0.01 M in CH_3CN) reference electrode at room temperature. Tetra-*n*-butylammonium hexafluorophosphate (0.1 M) was used as the supporting electrolyte. The redox potentials were recorded at a scan rate of 100 mV/s and are reported with reference to the ferrocene/ferrocenium (Fc/Fc^+) redox couple.

Theoretical Calculations. The geometries of the ground (S_0) and lowest-lying triplet excited (T_1) states of compounds were optimized using the density functional theory (DFT) method. The electronic transition energies including electron correlation effects were computed by the time-dependent density functional theory (TD-DFT)[39] method using the B3LYP[40] functional (TD-B3LYP). The 6-31G(d) basis set[41] was used for all atoms except for the Ir atom, which was treated with LANL2DZ effective core potentials (ECPs) and corresponding basis sets.[42] To include the solvation effects of THF,

dx.doi.org/10.1021/ic501286m | *Inorg. Chem.* 2014, 53, 8672−8680

the polarizable continuum model (PCM)[43] was used in the calculations. All calculations described here were carried out using the Gaussian 09 program.[44]

■ ASSOCIATED CONTENT

Supporting Information

X-ray crystallographic data for **5**, ^{1}H NMR spectra of **4**–**6**, fluoride titration results of **3** and **5**, PL spectra of **4** and **5** at 77 K, and computational details. This material is available free of charge via the Internet at http://pubs.acs.org.

■ AUTHOR INFORMATION

Corresponding Author

*E-mail: lmh74@ulsan.ac.kr.

Author Contributions

§These authors contributed equally.

Notes

The authors declare no competing financial interest.

■ ACKNOWLEDGMENTS

This work was supported by the Basic Science Research Program (NRF-2012R1A1A2039773 for M.H.L. and NRF-2013R1A1A2058722 for Y.H.L.) and Priority Research Centers Program (No. 2009-0093818), through the National Research Foundation of Korea (NRF) funded by the Ministry of Education. Y.S.L. acknowledges the financial support from the NRF (Nos. 2014-K1A3A1A09076 and 2007-0056341).

■ REFERENCES

(1) (a) Zhao, H.; Leamer, L. A.; Gabbaï, F. P. *Dalton Trans.* **2013**, *42*, 8164–8178. (b) Hudson, Z. M.; Wang, S. *Dalton Trans.* **2011**, *40*, 7805–7816. (c) Wade, C. R.; Broomsgrove, A. E. J.; Aldridge, S.; Gabbaï, F. P. *Chem. Rev.* **2010**, *110*, 3958–3984. (d) Jäkle, F. *Chem. Rev.* **2010**, *110*, 3985–4022. (e) Hudnall, T. W.; Chiu, C.-W.; Gabbaï, F. P. *Acc. Chem. Res.* **2009**, *42*, 388–397. (f) Hudson, Z. M.; Wang, S. *Acc. Chem. Res.* **2009**, *42*, 1584–1596. (g) Cametti, M.; Rissanen, K. *Chem. Commun.* **2009**, 2809–2829.

(2) Yamaguchi, S.; Akiyama, S.; Tamao, K. *J. Am. Chem. Soc.* **2001**, *123*, 11372–11375.

(3) (a) Song, K. C.; Lee, K. M.; Kim, H.; Lee, Y. S.; Lee, M. H.; Do, Y. *J. Organomet. Chem.* **2012**, *713*, 89–95. (b) Hudson, Z. M.; Liu, X.-Y.; Wang, S. *Org. Lett.* **2011**, *13*, 300–303.

(4) Wade, C. R.; Gabbaï, F. P. *Dalton Trans.* **2009**, 9169–9175.

(5) (a) Swamy P, C. A.; Thilagar, P. *Inorg. Chem.* **2014**, *53*, 2776–2786. (b) Lee, Y. H.; Nghia, N. V.; Go, M. J.; Lee, J.; Lee, S. U.; Lee, M. H. *Organometallics* **2014**, *33*, 753–762. (c) Sarkar, S. K.; Thilagar, P. *Chem. Commun.* **2013**, *49*, 8558–8560. (d) Song, K. C.; Kim, H.; Lee, K. M.; Lee, Y. S.; Do, Y.; Lee, M. H. *Sens. Actuators B* **2013**, *176*, 850–857. (e) Swamy P, C. A.; Mukherjee, S.; Thilagar, P. *Chem. Commun.* **2013**, *49*, 993–995. (f) Day, J. K.; Bresner, C.; Coombs, N. D.; Fallis, I. A.; Ooi, L.-L.; Aldridge, S. *Inorg. Chem.* **2008**, *47*, 793–804. (g) Liu, Z. Q.; Shi, M.; Li, F. Y.; Fang, Q.; Chen, Z. H.; Yi, T.; Huang, C. H. *Org. Lett.* **2005**, *7*, 5481–5484. (h) Yamaguchi, S.; Shirasaka, T.; Akiyama, S.; Tamao, K. *J. Am. Chem. Soc.* **2002**, *124*, 8816–8817.

(6) Sun, Y.; Wang, S. *Inorg. Chem.* **2009**, *48*, 3755–3767.

(7) Liu, X. Y.; Bai, D. R.; Wang, S. *Angew. Chem., Int. Ed.* **2006**, *45*, 5475–5478.

(8) Zhao, Q.; Li, F.; Huang, C. *Chem. Soc. Rev.* **2010**, *39*, 3007–3030.

(9) You, Y.; Park, S. Y. *Adv. Mater.* **2008**, *20*, 3820–3826.

(10) (a) Ko, S.-B.; Lu, J.-S.; Kang, Y.; Wang, S. *Organometallics* **2013**, *32*, 599–608. (b) Blight, B. A.; Stewart, A. F.; Wang, N.; Lu, J.-s.; Wang, S. *Inorg. Chem.* **2012**, *51*, 778–780. (c) Sun, Y.; Hudson, Z. M.; Rao, Y.; Wang, S. *Inorg. Chem.* **2011**, *50*, 3373–3378. (d) Sun, Y.; Wang, S. *Inorg. Chem.* **2010**, *49*, 4394–4404. (e) Wade, C. R.; Gabbaï, F. P. *Inorg. Chem.* **2010**, *49*, 714–720. (f) Hudson, Z. M.; Zhao, S.-B.; Wang, R.-Y.; Wang, S. *Chem.—Eur. J.* **2009**, *15*, 6131–6137. (g) Rao, Y.-L.; Wang, S. *Inorg. Chem.* **2009**, *48*, 7698–7713. (h) Lam, S.-T.; Zhu, N.; Yam, V. W.-W. *Inorg. Chem.* **2009**, *48*, 9664–9670. (i) Sun, Y.; Ross, N.; Zhao, S.-B.; Huszarik, K.; Jia, W.-L.; Wang, R.-Y.; Macartney, D.; Wang, S. *J. Am. Chem. Soc.* **2007**, *129*, 7510–7511. (j) Zhao, S.-B.; McCormick, T.; Wang, S. *Inorg. Chem.* **2007**, *46*, 10965–10967. (k) Sakuda, E.; Funahashi, A.; Kitamura, N. *Inorg. Chem.* **2006**, *45*, 10670–10677. (l) Melaïmi, M.; Gabbaï, F. P. *J. Am. Chem. Soc.* **2005**, *127*, 9680–9681.

(11) (a) Li, Y.; Hyun, M. H. *Bull. Korean Chem. Soc.* **2011**, *32*, 4125–4128. (b) Zhao, Q.; Li, F.; Liu, S.; Yu, M.; Liu, Z.; Yi, T.; Huang, C. *Inorg. Chem.* **2008**, *47*, 9256–9264.

(12) Xu, W.-J.; Liu, S.-J.; Zhao, X.-Y.; Sun, S.; Cheng, S.; Ma, T.-C.; Sun, H.-B.; Zhao, Q.; Huang, W. *Chem.—Eur. J.* **2010**, *16*, 7125–7133.

(13) (a) Chi, Y.; Chou, P.-T. *Chem. Soc. Rev.* **2010**, *39*, 638–655. (b) You, Y.; Park, S. Y. *Dalton Trans.* **2009**, 1267–1282. (c) Flamigni, L.; Barbieri, A.; Sabatini, C.; Ventura, B.; Barigelletti, F. *Top. Curr. Chem.* **2007**, *281*, 143–203. (d) Chou, P.-T.; Chi, Y. *Chem.—Eur. J.* **2007**, *13*, 380–395. (e) Ma, B.; Djurovich, P. I.; Thompson, M. E. *Coord. Chem. Rev.* **2005**, *249*, 1501–1510. (f) Yersin, H. *Top. Curr. Chem.* **2004**, *241*, 1–26.

(14) Xu, W.; Liu, S.; Sun, H.; Zhao, X.; Zhao, Q.; Sun, S.; Cheng, S.; Ma, T.; Zhou, L.; Huang, W. *J. Mater. Chem.* **2011**, *21*, 7572–7581.

(15) Vadavi, R. S.; Kim, H.; Lee, K. M.; Kim, T.; Lee, J.; Lee, Y. S.; Lee, M. H. *Organometallics* **2012**, *31*, 31–34.

(16) (a) Li, H.; Lalancette, R. A.; Jäkle, F. *Chem. Commun.* **2011**, *47*, 9378–9380. (b) Kim, Y.; Huh, H.-S.; Lee, M. H.; Lenov, I. L.; Zhao, H.; Gabbaï, F. P. *Chem.—Eur. J.* **2011**, *17*, 2057–2062.

(17) Voronkov, A.; Holsworth, D. D.; Waaler, J.; Wilson, S. R.; Ekblad, B.; Perdreau-Dahl, H.; Dinh, H.; Drewes, G.; Hopf, C.; Morth, J. P.; Krauss, S. *J. Med. Chem.* **2013**, *56*, 3012–3023.

(18) Jia, W.-L.; Bai, D.-R.; McCormick, T.; Liu, Q.-D.; Motala, M.; Wang, R.-Y.; Seward, C.; Tao, Y.; Wang, S. *Chem.—Eur. J.* **2004**, *10*, 994–1006.

(19) (a) Tamayo, A. B.; Alleyne, B. D.; Djurovich, P. I.; Lamansky, S.; Tsyba, I.; Ho, N. N.; Bau, R.; Thompson, M. E. *J. Am. Chem. Soc.* **2003**, *125*, 7377–7387. (b) Schmid, B.; Garces, F. O.; Watts, R. J. *Inorg. Chem.* **1994**, *33*, 9–14.

(20) Lamansky, S.; Djurovich, P.; Murphy, D.; Abdel-Razzaq, F.; Kwong, R.; Tsyba, I.; Bortz, M.; Mui, B.; Bau, R.; Thompson, M. E. *Inorg. Chem.* **2001**, *40*, 1704–1711.

(21) Sajoto, T.; Djurovich, P. I.; Tamayo, A. B.; Oxgaard, J.; Goddard, W. A.; Thompson, M. E. *J. Am. Chem. Soc.* **2009**, *131*, 9813–9822.

(22) Lamansky, S.; Djurovich, P.; Murphy, D.; Abdel-Razzaq, F.; Lee, H. E.; Adachi, C.; Burrows, P. E.; Forrest, S. R.; Thompson, M. E. *J. Am. Chem. Soc.* **2001**, *123*, 4304–4312.

(23) Baranoff, E.; Curchod, B. F. E.; Monti, F.; Steimer, F.; Accorsi, G.; Tavernelli, I.; Rothlisberger, U.; Scopelliti, R.; Grätzel, M.; Nazeeruddin, M. K. *Inorg. Chem.* **2012**, *51*, 799–811.

(24) Xu, M.; Zhou, R.; Wang, G.; Xiao, Q.; Du, W.; Che, G. *Inorg. Chim. Acta* **2008**, *361*, 2407–2412.

(25) Huh, J. O.; Kim, H.; Lee, K. M.; Lee, Y. S.; Do, Y.; Lee, M. H. *Chem. Commun.* **2010**, *46*, 1138–1140.

(26) (a) Kim, Y.; Gabbaï, F. P. *J. Am. Chem. Soc.* **2009**, *131*, 3363–3369. (b) Solé, S.; Gabbaï, F. P. *Chem. Commun.* **2004**, 1284–1285.

(27) (a) Hudnall, T. W.; Gabbaï, F. P. *J. Am. Chem. Soc.* **2007**, *129*, 11978–11986. (b) Yuan, Z.; Entwistle, C. D.; Collings, J. C.; Albesa-Jové, D.; Batsanov, A. S.; Howard, J. A. K.; Taylor, N. J.; Kaiser, H. M.; Kaufmann, D. E.; Poon, S.-Y.; Wong, W.-Y.; Jardin, C.; Fathallah, S.; Boucekkine, A.; Halet, J.-F.; Marder, T. B. *Chem.—Eur. J.* **2006**, *12*, 2758–2771.

(28) Lee, M. H.; Agou, T.; Kobayashi, J.; Kawashima, T.; Gabbaï, F. P. *Chem. Commun.* **2007**, 1133–1135.

(29) Rausch, A. F.; Thompson, M. E.; Yersin, H. *J. Phys. Chem. A* **2009**, *113*, 5927–5932.

(30) Gupta, D.; Katiyar, M.; Deepak; Hazra, T.; Verma, A.; Manoharan, S. S.; Biswas, A. *Opt. Mater.* **2006**, *28*, 1355–1361.

(31) Sie, W.-S.; Jian, J.-Y.; Su, T.-C.; Lee, G.-H.; Lee, H. M.; Shiu, K.-B. *J. Organomet. Chem.* **2008**, *693*, 1510−1517.
(32) (a) Xu, M.; Zhou, R.; Wang, G.; Yu, J. *Inorg. Chim. Acta* **2009**, *362*, 2183−2188. (b) You, Y.; Kim, K. S.; Ahn, T. K.; Kim, D.; Park, S. Y. *J. Phys. Chem. C* **2007**, *111*, 4052−4060. (c) You, Y.; Park, S. Y. *J. Am. Chem. Soc.* **2005**, *127*, 12438−12439.
(33) Baranoff, E.; Curchod, B. F. E.; Frey, J.; Scopelliti, R.; Kessler, F.; Tavernelli, I.; Rothlisberger, U.; Grätzel, M.; Nazeeruddin, M. K. *Inorg. Chem.* **2012**, *51*, 215−224.
(34) (a) You, Y.; An, C.-G.; Kim, J.-J.; Park, S. Y. *J. Org. Chem.* **2007**, *72*, 6241−6246. (b) Tsuboyama, A.; Iwawaki, H.; Furugori, M.; Mukaide, T.; Kamatani, J.; Igawa, S.; Moriyama, T.; Miura, S.; Takiguchi, T.; Okada, S.; Hoshino, M.; Ueno, K. *J. Am. Chem. Soc.* **2003**, *125*, 12971−12979.
(35) Orselli, E.; Kottas, G. S.; Konradsson, A. E.; Coppo, P.; Fröhlich, R.; De Cola, L.; van Dijken, A.; Büchel, M.; Börner, H. *Inorg. Chem.* **2007**, *46*, 11082−11093.
(36) Kolosov, D.; Adamovich, V.; Djurovich, P.; Thompson, M. E.; Adachi, C. *J. Am. Chem. Soc.* **2002**, *124*, 9945−9954.
(37) Yeh, Y.-S.; Cheng, Y.-M.; Chou, P.-T.; Lee, G.-H.; Yang, C.-H.; Chi, Y.; Shu, C.-F.; Wang, C.-H. *ChemPhysChem* **2006**, *7*, 2294−2297.
(38) Sheldrick, G. M. *SHELXL-93: Program for the Refinement of Crystal Structures*; University of Göttingen: Göttingen, Germany, 1993.
(39) Runge, E.; Gross, E. K. U. *Phys. Rev. Lett.* **1984**, *52*, 997−1000.
(40) (a) Stephens, P. J.; Devlin, F. J.; Chabalowski, C. F.; Frisch, M. J. *J. Phys. Chem.* **1994**, *98*, 11623−11627. (b) Lee, C.; Yang, W.; Parr, R. G. *Phys. Rev. B* **1988**, *37*, 785−789.
(41) (a) Francl, M. M.; Pietro, W. J.; Hehre, W. J.; Binkley, J. S.; Gordon, M. S.; DeFrees, D. J.; Pople, J. A. *J. Chem. Phys.* **1982**, *77*, 3654−3665. (b) Hariharan, P. C.; Pople, J. A. *Theoret. Chim. Acta.* **1973**, *28*, 213−222. (c) Hehre, W. J.; Ditchfield, R.; Pople, J. A. *J. Chem. Phys.* **1972**, *56*, 2257−2261.
(42) Hay, P. J.; Wadt, W. R. *J. Chem. Phys.* **1985**, *82*, 270−283.
(43) (a) Mennucci, B.; Tomasi, J.; Cammi, R.; Cheeseman, J. R.; Frisch, M. J.; Devlin, F. J.; Gabriel, S.; Stephens, P. J. *J. Phys. Chem. A* **2002**, *106*, 6102−6113. (b) Cammi, R.; Tomasi, J. *J. Comput. Chem.* **1995**, *16*, 1449−1458. (c) Miertuš, S.; Scrocco, E.; Tomasi, J. *Chem. Phys.* **1981**, *55*, 117−129.
(44) Frisch, M. J.; Trucks, G. W.; Schlegel, H. B.; Scuseria, G. E.; Robb, M. A.; Cheeseman, J. R.; Montgomery, J. A. Jr.; Vreven, T.; Kudin, K. N.; Burant, J. C.; Millam, J. M.; Iyengar, S. S.; Tomasi, J.; Barone, V.; Mennucci, B.; Cossi, M.; Scalmani, G.; Rega, N.; Petersson, G. A.; Nakatsuji, H.; Hada, M.; Ehara, M.; Toyota, K.; Fukuda, R.; Hasegawa, J.; Ishida, M.; Nakajima, T.; Honda, Y.; Kitao, O.; Nakai, H.; Klene, M.; Li, X.; Knox, J. E.; Hratchian, H. P.; Cross, J. B.; Bakken, V.; Adamo, C.; Jaramillo, J.; Gomperts, R.; Stratmann, R. E.; Yazyev, O.; Austin, A. J.; Cammi, R.; Pomelli, C.; Ochterski, J. W.; Ayala, P. Y.; Morokuma, K.; Voth, G. A.; Salvador, P.; Dannenberg, J. J.; Zakrzewski, V. G.; Dapprich, S.; Daniels, A. D.; Strain, M. C.; Farkas, O.; Malick, D. K.; Rabuck, A. D.; Raghavachari, K.; Foresman, J. B.; Ortiz, J. V.; Cui, Q.; Baboul, A. G.; Clifford, S.; Cioslowski, J.; Stefanov, B. B.; Liu, G.; Liashenko, A.; Piskorz, P.; Komaromi, I.; Martin, R. L.; Fox, D. J.; Keith, T.; Al-Laham, M. A.; Peng, C. Y.; Nanayakkara, A.; Challacombe, M.; Gill, P. M. W.; Johnson, B.; Chen, W.; Wong, M. W.; Gonzalez, C.; Pople, J. A. *Gaussian 09, Revision A.02*; Gaussian, Inc.: Wallingford, CT, 2009.

■ NOTE ADDED AFTER ASAP PUBLICATION

This paper was published on the Web on August 4, 2014, with minor text errors throughout the paper. The corrected version was reposted on August 5, 2014.